J Mater Sci (2020) 55:14858–14872

Computation & theory

Atomistic insight into shell–core evolution of aluminum nanoparticles in reaction with gaseous oxides at high temperature

Liang Song[1], Si-Yu Xu[2], Feng-Qi Zhao[2], and Xue-Hai Ju[1,*]

[1] Key Laboratory of Soft Chemistry and Functional Materials of MOE, School of Chemical Engineering, Nanjing University of Science and Technology, Nanjing 210094, People's Republic of China

[2] Science and Technology on Combustion and Explosion Laboratory, Xi'an Modern Chemistry Research Institute, Xi'an 710065, People's Republic of China

Received: 24 March 2020
Accepted: 7 July 2020
Published online: 20 July 2020

ABSTRACT

Aluminum nanoparticles (ANPs), as an economical and effective metal fuel, are widely applied in energetic formulations. The objective of this research was to gain insights into the oxidation of ANPs in gaseous oxides (CO_2, CO, NO_2, and NO). The reactive molecular dynamics (RMD) simulations were performed to elucidate the detailed mechanisms of surface oxidation, chain-like products formation, and hollow formation in the evolution of ANPs. The O atoms in gaseous oxides are adsorbed on the ANPs' surface followed by the cleavage of O–C/N bond. The nucleation and growth of chain-like products occur in dense gaseous oxides. The four forms of chain products include tilted chain, twisted chain, branched chain, and cyclic chain were observed in CO atmosphere. A similar chain structure is also formed in NO atmosphere, but the chain length is significantly reduced. The oxide shell of ANPs is formed and expands rapidly in CO_2 atmosphere, resulting in voids between oxide shell and Al core. Al atoms are transported from the core to the oxide shell through a bridge composed of Al atoms. The Al core gradually diffused outward and was eventually hollowed out. In addition, the final product has carbon deposits (C_{48} and C_{98}) on the surface and core.

Address correspondence to E-mail: xhju@njust.edu.cn

https://doi.org/10.1007/s10853-020-05062-y

GRAPHICAL ABSTRACT

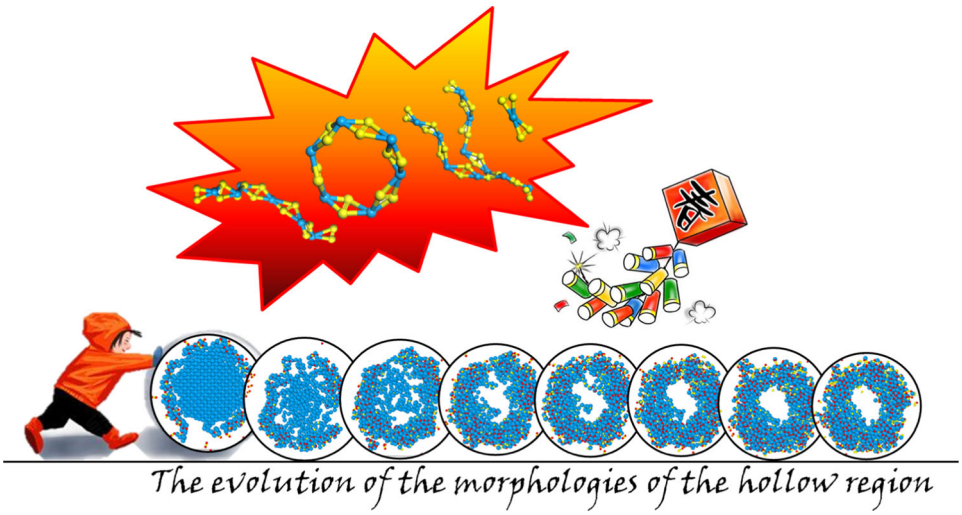

Introduction

Metal powders that can transiently release a large quantity of combustion heat by oxidation are widely used as propellants and fuels [1–3]. Currently, aluminum powder has been recognized as one of the ideal energetic metals due to its high energy density, abundant raw materials, and environmentally friendly combustion products [4, 5]. However, the oxide films on aluminum powder have significant impacts on its ignition. The alumina layer will reduce the energy release of aluminum combustion [6]. To improve these problems, aluminum nanoparticles (ANPs) with higher activity are used to replace the micro-sized ones because of its specific properties, such as size effect and surface-interface effect [7–10]. Meda et al. used scanning electron microscopy, specific surface area measurements, X-ray photoelectron spectroscopy, and X-ray diffraction to study the combustion characteristics of nano-aluminum powder in solid propellants. It was found that the combustion efficiency of the propellant containing nanoparticles was significantly improved, and the smaller the particle size of the aluminum powder, the lower the ignition temperature of the propellant and the shorter the combustion time [11]. Meda et al. also tested the content of unburned aluminum powder in the combustion products of solid propellants. It is found that the content of unburned aluminum powder in the combustion products of nano-aluminum powder is lower than that of micron powder [12]. Ivanov et al. also found that the burning rate of Alex propellants (an ultra-fine aluminum powder produced by plasma explosion process) is higher than that of ordinary micron aluminum powder propellants [13].

The atomic insights into the ignition mechanism of ANPs have been investigated in the extremely small scales of space and time [14, 15]. Hong et al. studied the oxidation mechanism of ANPs by using ReaxFF molecular dynamics simulations. It is proposed that the ANPs oxidation depends on combined effects of the temperature and the oxygen gas pressure [15]. Campbell et al. determined that the large pressure gradients exist inside the oxidized ANPs by using the molecular dynamics simulations. The results indicated that the aluminum core is in positive pressure, while the oxide shell is under negative pressure [16, 17]. However, most previous researches on ignition of ANPs have been performed in oxygen atmosphere, and only a few studies have been performed to investigate the ignition of ANPs in other atmospheres. Actually, ignition and combustion of

ANPs under various conditions are also of significance. Carbon oxides and nitrogen oxides are the main components of solid rocket propellant combustion products that can interact with metal aluminum powder. Furthermore, it is well known that Martian atmosphere contains about 96% of CO_2, which makes it possible to achieve in situ resource utilization. Therefore, the Al/CO_2 mixture is considered a promising fuel for future Mars exploration missions. Palopoli et al. studied the pyrolysis gaseous products of nitramine compounds and found that these gas products contained a large amount of nitrogen oxides such as N_2O, NO_2, NO [18]. Yan et al. found that a large amount of nitrogen oxides are emitted during the combustion of nitramine propellants. It is of great significance to study the effect of these nitrogen oxides on aluminum oxidation, especially the exploration of the combustion mechanism of high-energy solid fuels [19]. Therefore, in the combustion of aluminum-based fuels, it is of great importance to study the interaction between gaseous molecules and aluminum, especially to explore the combustion mechanism of high-energy solid fuel propellants. Meanwhile, keeping ANPs stable under various conditions of manufacture, transportation, stock, and application is also of significance. Therefore, the detailed understanding of the transient structure evolution of ANPs as well as its interplay with the small gaseous molecules at the ignition stage is very meaningful. In this work, we performed reactive molecular dynamics (RMD) simulations to show the ignition of ANPs in four different atmospheres (CO_2, CO, NO_2, and NO). Our results would provide important insights into understanding the initial ignition and combustion mechanisms of metallic nanoparticles.

Computational details

The reactive force field (ReaxFF), developed and trained from quantum mechanical calculations, employs connectivity, bond-order formalism and polarizable charge descriptions to compute precisely both reactive and non-reactive interactions [20–24]. In this study, a ReaxFF suitable for ANP was applied to investigate the ignition and combustion mechanism of ANP under four gaseous oxides [25]. The ANP structure (Al_{3997}, 5.0 nm in diameter) was established and placed at the center of the simulation box measured 10.1 × 10.1 × 10.1 nm by using the materials visualizer tool. Different atmospheres were randomly filled into the remaining empty spaces in the box. To study the effect of gas pressure on ignition and combustion, the low density, medium density, and high density for each gas were filled in boxes. Details on the four gaseous oxides are listed in Table 1. The thickness of the vacuum layer between ANP and gases component was set as 0.2 nm. The models were equilibrated at 298 K for 10 ps and then were heated rapidly to the target temperatures within 30 ps, and were equilibrated finally at target temperatures for 200 ps. We performed the RMD simulations in the canonical (NVT) ensemble using the Nosé–Hoover thermostat [26, 27]. These initial model settings were repeated infinitely by imposing periodic boundary conditions in all three dimensions. The detailed information of dynamic trajectory was recorded every 50 fs and applied to analyze the evolution of ANP at five temperatures (1500, 2000, 2500, 3000, and 3500 K). The initial atomic velocities based on the required temperatures in different systems were determined according to the Maxwell–Boltzmann distribution. Newton's equation of motion was calculated using the velocity Verlet algorithm with a time step of 0.1 fs, and atomic charges were obtained by the charge equilibration (QEq) method with the update of each 10th time step. All RMD simulations were performed using large-scale atomic/molecular massively parallel simulator (LAMMPS) program package [28].

Results and discussion

Dynamic morphologies of ANPs

To investigate the reaction mechanism of CO_2 oxidation, the evolution of the charge distribution is shown in Fig. 1. At 0 ps, the charge of Al atoms tends to be zero. When it reaches 20 ps (heating stage), CO_2 molecules move to and react with Al atoms on the surface of ANPs. With the prolonged heating time, the low-coordinated Al transitions to the high-coordinated oxide, and the oxide gradually grows to the inside of ANP. In addition, the higher the density of CO_2, the more intense the oxidation reaction. The large pressure gradients accumulate inside the oxide at this time. The generation of staggered stress fields causes the nanoparticle shape to change. Therefore,

Table 1 The number of molecules of the filling gas and the corresponding gaseous density (g/cm^3)

Atmospheres	Number of molecules/density (low)	Number of molecules/density (medium)	Number of molecules/density (high)
CO_2	690/0.055	1380/0.11	2770/0.22
CO	690/0.035	1380/0.07	2770/0.14
NO_2	690/0.058	1380/0.115	2770/0.23
NO	690/0.0375	1380/0.075	2770/0.15

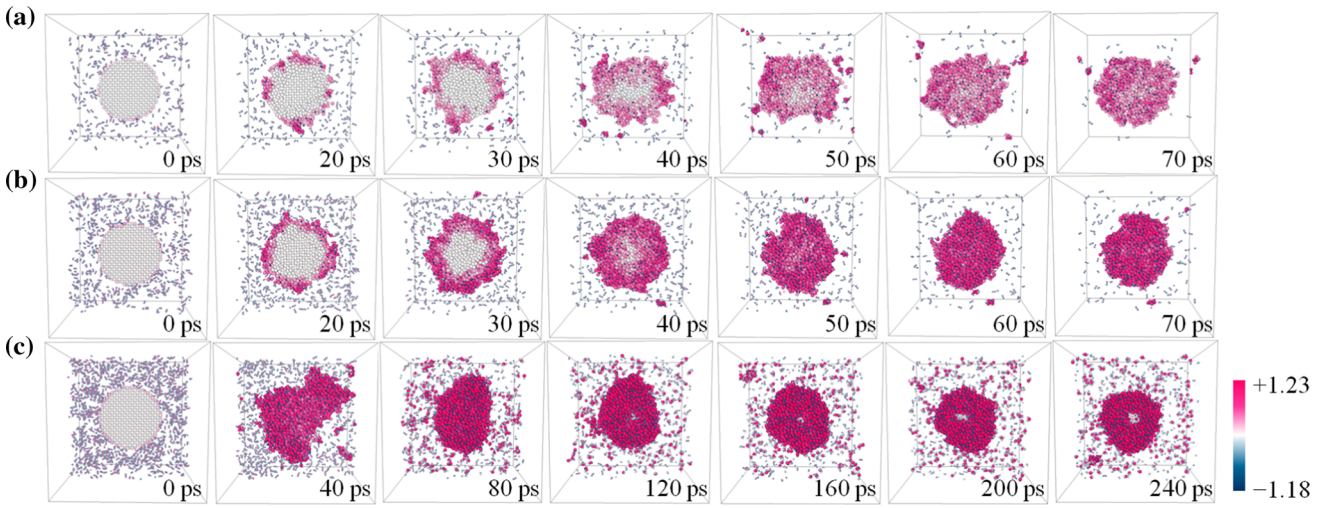

Figure 1 Evolution of charge distribution of ANPs–CO_2 systems with time at 3500 K. The CO_2 densities of **a** 0.055 g/cm^3, **b** 0.11 g/cm^3, and **c** 0.22 g/cm^3 were selected as examples.

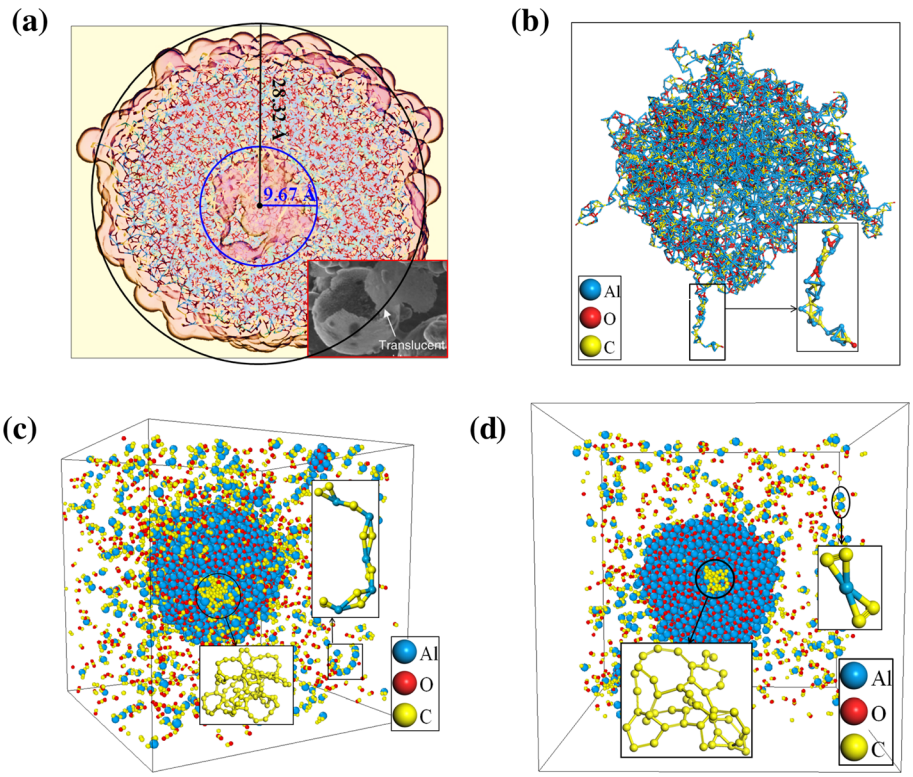

Figure 2 **a** The cross section images of Connolly surface area of the solid, the hollow cavity with a radius of 9.67 A in the particles (240 ps). Thumbnail image of cavity of 3-μm Al in the bottom right [31]. **b** The nanoparticle shape of the solid region at 2000 K (40 ps). **c** Surface carbon deposition of nanoparticles and external long chain of Al_5C_{12}. **d** Core carbon deposition of nanoparticles (sectional drawing). The blue, red and yellow atoms represent the Al, O and C atoms, respectively.

when the density of CO_2 is 0.22 g/cm^3, the nanoparticles could not maintain the spherical morphology at 40 ps.

The Connolly surface defines the boundary between the solid area and its environment. The Connolly surface calculations were obtained by atom volumes and surfaces (Material studio, version 6.0). Figure 2a shows the hollow oxide spheres in the oxidation reaction of ANPs and CO_2 with a density of 0.22 g/cm^3 at 1500 K. By calculating the Connolly surface, the radius and area of the hollow region are 9.67 Å and 2.885 nm^2, respectively. Hollow structures have been reported by researchers [29–31]. They proposed the oxide developed on the shell of the sphere. The new phase expanded around the exterior as temperature increased. The presence of hollow structures is because outward Al diffusion has resulted in a core hollow. The evolution of hollow region is shown in Fig. 3. The thin slices with a thickness of 0.5 nm show the details of the internal structural evolution. The initial reaction mainly occurred in the surface area. The oxidation of the surface causes the atoms to rearrange and to release a large amount of heat. The oxide shell rapidly expands and grows into the outer space, causing a significant void between oxide shell and the Al core. At 40 ps, Al atoms diffuse and form clusters in the void. The Al core and the oxide shell are connected by some bridges composed of Al atoms. The Al core transport Al atoms to the oxide shell through them, which promoted further oxidation of Al in oxide shell. The Al atoms in the core gradually diffused outward and was eventually hollowed out. Hence there is a big central void in the final nanoparticle product. Chakraborty et al. studied the diffusion mechanism of oxide-coated ANPs at 2000 K. Hollow particles are considered to be in a transient state and can be considered to the higher outward diffusion of aluminum ions compared to the inward diffusion of the shell ions [29]. Figure 2b shows the nanoparticle shape of the same system at 2000 K. Both the surface and internal structure of ANPs undergo significant changes in CO_2 oxidation and generate a large number of defects. Due to the misfit dislocations on the surface and the emission of atomic chain oxides, the ANPs are more conducive to being oxidized by CO_2 [32]. Sarou et al. observed the carbon dissolution process in combustion of Al–CO_2. The carbon concentration reached the saturation limit ($x_C = 0.23$ at $T = 2600$ K), the excess carbon was ejected on the surface and formed a solid coating [33]. Carbon coats the aluminum surface to suppress the burning of aluminum. C deposits are easily formed under high-temperature reactions. Some results further confirm carbon deposition [31, 33, 34]. Figure 2c illustrates the formation of C_{98} deposited on the nanoparticle surface at 2000 K. At the same time, a chain-like product is generated in a gaseous environment. The chemical formula of long chain is Al_5C_{12}, and the C≡C and $^{[4]}$Al are arranged alternately, and the starting and ending ends are C≡C. In addition to carbon surface deposition, there is also internal carbon deposition.

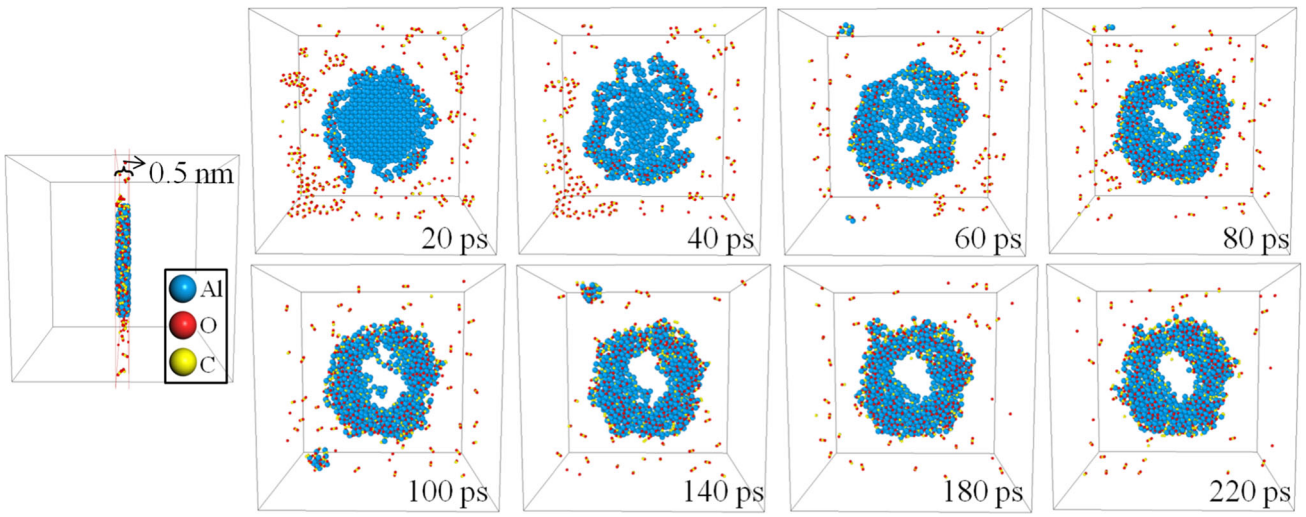

Figure 3 The evolution of the morphologies of the hollow region at 1500 K. The blue, red and yellow atoms represent the Al, O and C atoms, respectively.

As shown in Fig. 2d, C48 exists at the core of the nanoparticles at 3500 K. As the nanoparticles are fully oxidized at high temperatures, agglomeration occurs between the same phases. Most C atoms in the nanoparticles move outward and accumulate on the surface, and the other part of the C atoms move inward. Eventually, these C atoms are mainly distributed on the core or surface of the nanoparticles. The possibility of forming C deposits on the surface or core is greater. As the aluminum oxide expands outward, the stress inside the nanoparticles is reduced, and the inward C atoms aggregate into C deposits such as C_{98} and C_{48}. The presence of a large amount of AlC_4 in the gaseous environment indicates that high temperature is not conducive to the growth of the Al_nC_{2n+2} chain.

Compared with the combustion of ANPs–CO_2, the severity of ANPs–CO combustion was significantly reduced. Similarly, taking three CO densities at 3500 K as an example, the evolution of charge distribution of ANPs are shown in Fig. 4. When the CO densities are 0.035 g/cm^3 and 0.07 g/cm^3, ANPs oxidized from the shell to the core. The ANPs are not completely oxidized due to the limitation of the oxygen concentration in the external atmosphere. When the CO density reaches 0.14 g/cm^3, the oxidation of ANPs increases significantly. In addition, the thermal energy released by the surface reactions could trigger greater stress on the oxide coating, causing the oxide of the shell to be broken down at 40 ps. In addition, the chain-like product in the atmosphere environment gradually nucleates and grows from 120 to 240 ps.

Figure 5a shows the interaction of CO molecules with ANPs in the initial heating stage. Since the electronegetivity of oxygen is much greater than that of carbon, the CO molecules adjacent ANPs adjust their orientation so that the O-terminal faces ANPs. Figure 5b shows chain oxides ejecting out from the nanoparticles. The chain product is composed of repeated Al_4O, and its core consists of oxygen atoms and is externally bonded with four Al, which damages the oxide layer and facilitates further oxidation. The chain-like nucleation and growth of oxides were observed on the ANPs surface during the oxidation and microexplosion-accelerated oxidation [32, 35]. Our results demonstrated these viewpoints further. Figure 5c shows a snapshot of the ANPs–CO system with the CO density is 0.14 g/cm^3. There are a lot of carbon-containing chain products in the ANPs–CO system, far more than the ANPs–CO_2 system. This is mainly due to the increase in the relative concentration of C. Four forms of chain products including tiled chain (I), twisted chain (II), branched chain (III), and cyclic chain (IV) were observed. The chemical formula of tiled chain (I), twisted chain (II) and branched chain (III) is Al_nC_{2n+2}, and that of the cyclic chain (IV) is Al_nC_{2n}.

Figure 6a shows the morphological evolution of ANPs in NO_2 atmosphere. The ambient atmosphere was composed of NO_2 at first, and the amount of N_2 formed increased significantly with time. Figure 6b

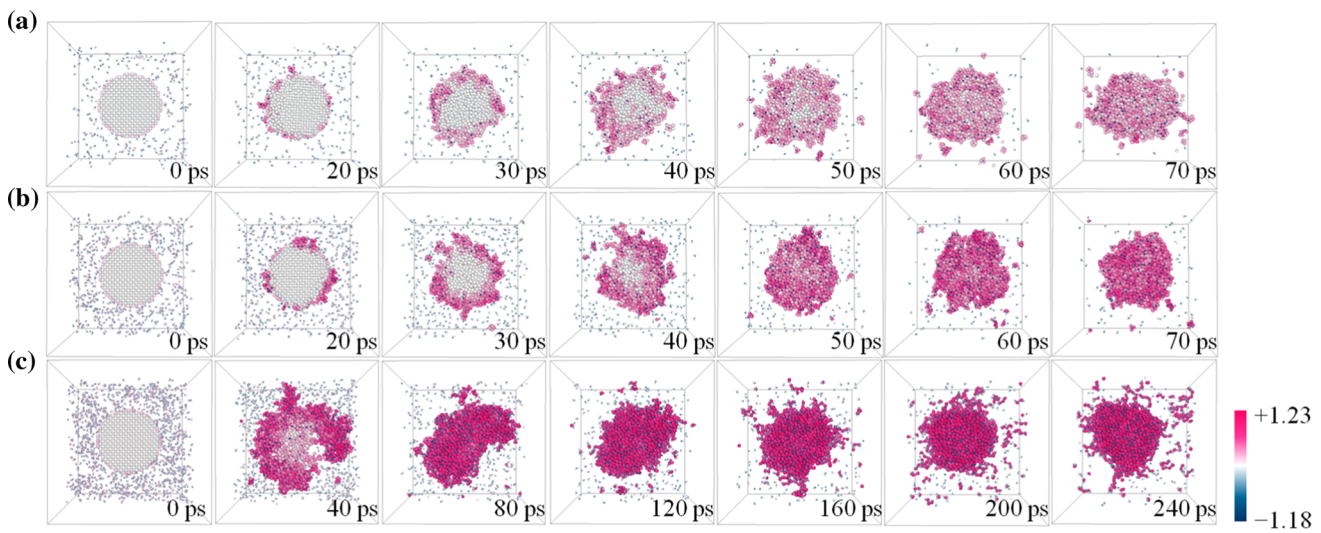

Figure 4 Evolution of charge distribution of ANPs–CO systems with time at 3500 K. The CO densities of **a** 0.035 g/cm^3, **b** 0.07 g/cm^3, and **c** 0.14 g/cm^3.

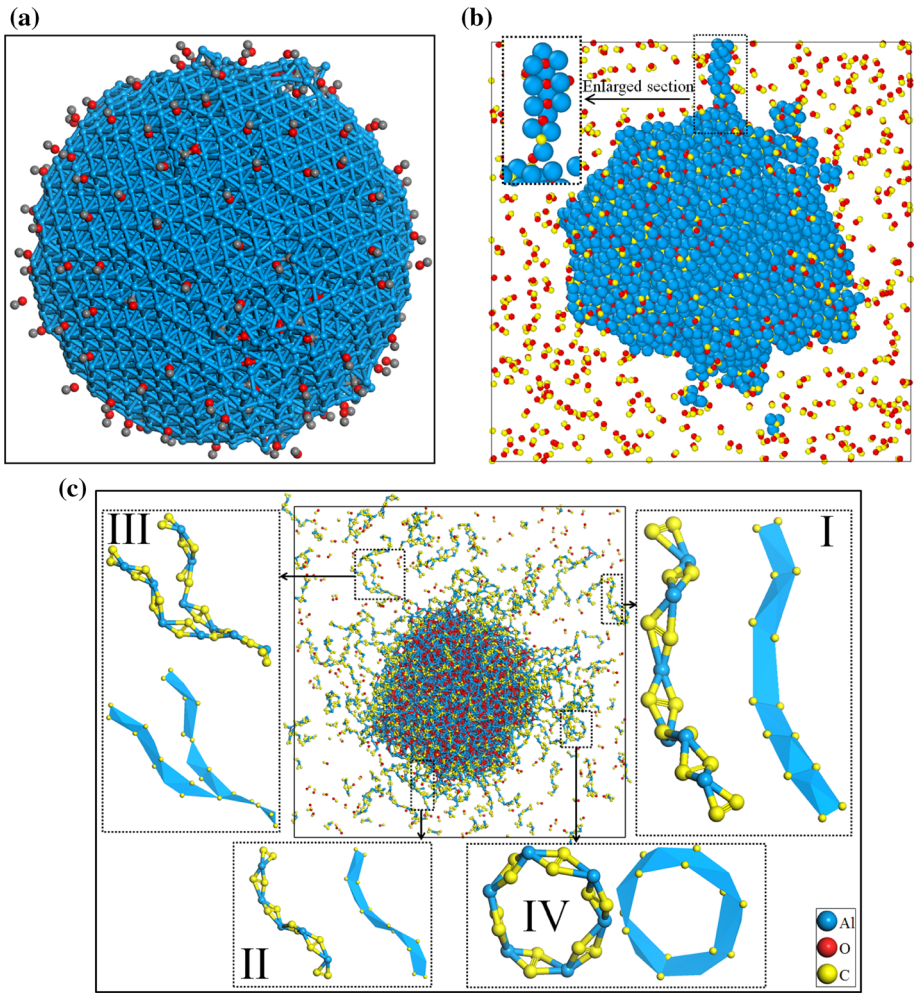

Figure 5 **a** The interaction between CO molecules and ANPs in the range of 0.2 nm when the density of CO in the environment is 0.035 g/cm^3. **b** The snapshot of the nanoparticles when the CO density is 0.07 g/cm^3. The enlarged view is a cross-sectional view of the chain ejected by the nanoparticles. **c** The snapshot of the system at 3500 K with a CO density of 0.14 g/cm^3. The enlarged ball–stick skeleton and polyhedron diagrams are Al_6C_{14} (I), Al_5C_{12} (II), $Al_{10}C_{22}$ (III) and Al_6C_{12} (IV), respectively.

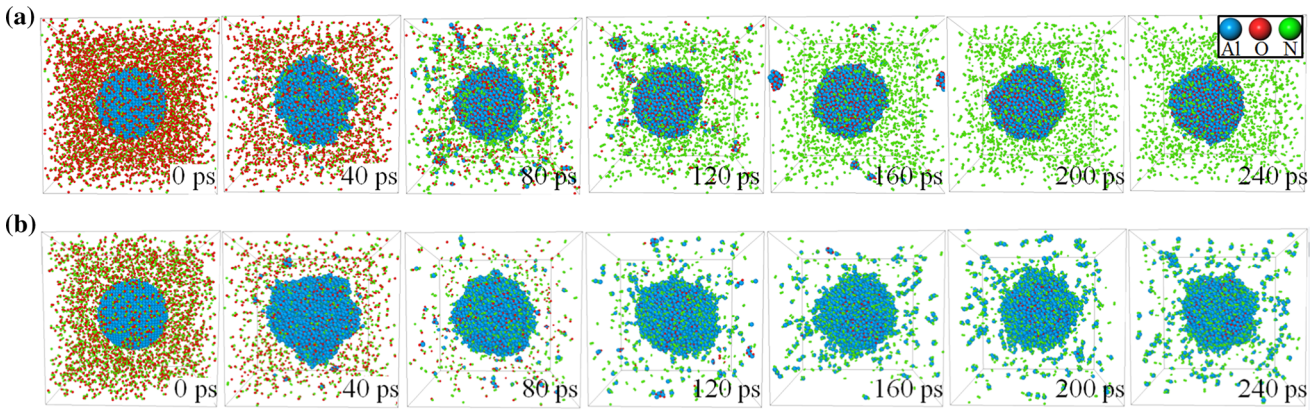

Figure 6 Morphological evolutions of ANPs in the **a** nitrogen dioxide and **b** nitric oxide with the densities of 0.23 g/cm^3 and 0.15 g/cm^3, respectively. Blue, red and green represent Al, O and N atoms, respectively.

shows the morphological evolution of ANPs in NO atmosphere. Consistent with the reaction of ANPs–NO_2, oxygen in NO as the main component participates in the reaction with ANPs. The difference is the distribution of aluminum nitride clusters that increase with time in the external environment. Although the density of NO_2 and NO is different, the molecular numbers of two are the same. What causes

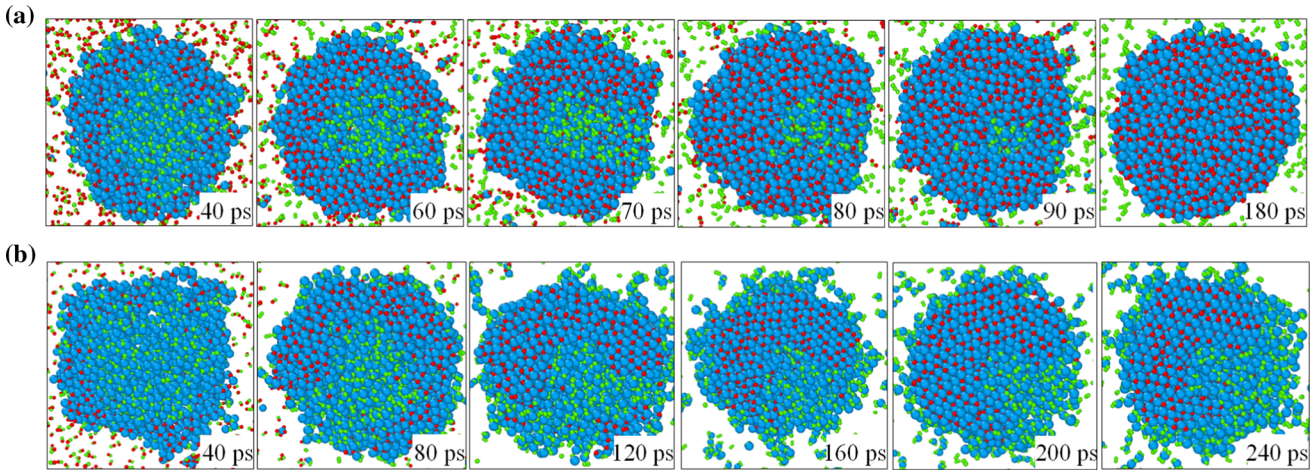

Figure 7 Sectional view of nanoparticle evolution in **a** NO_2 and **b** NO atmosphere. Blue, red and green represent Al, O and N atoms, respectively.

the difference in the final ambient gas? The cross-sectional drawings of the nanoparticles in the reaction are showed in Fig. 7. It is found from the RMD trajectory that N diffuses faster than O in ANPs. In the early stage, although aluminum oxide was formed and remained in the shell, N atoms were not hindered and diffused to the center of the nanoparticle first. Driven by thermodynamics, Al–O bond formation is more favorable at high temperature. Therefore, the O atoms gradually replace N atoms in the nitride phase of nanoparticles. For the ANPs–NO_2 system, we observe a clear phenomenon of competition between oxide phase and nitride phase from 60 to 80 ps. The oxide phase expands and the nitride phase continuously disappears in the ANPs–NO_2 system. The formation of an aluminum oxide cap moves on the particle surface in the combustion experiment [36]. Our simulation results are consistent with experimental phenomena. We found that the aluminum nitride clusters in the environmental phase increase significantly during this period, as shown in the snapshot of 80 ps in Fig. 6a. Because the boiling point of Al_2O_3 (2980 °C) is higher than the melting point of AlN (2249 °C), the aluminum nitride easily enters the environmental phase as a gaseous molecule. For the ANPs–NO system, the concentration of O is not sufficient to oxidize completely the ANPs. As a result, significant phase separation and phase agglomeration occur. Small aluminum nitride clusters are released into the environmental phase continuously because of the lower-boiling aluminum nitride. Figure 8 shows a snapshot of the ANPs–NO system. There are a large number of chain products in

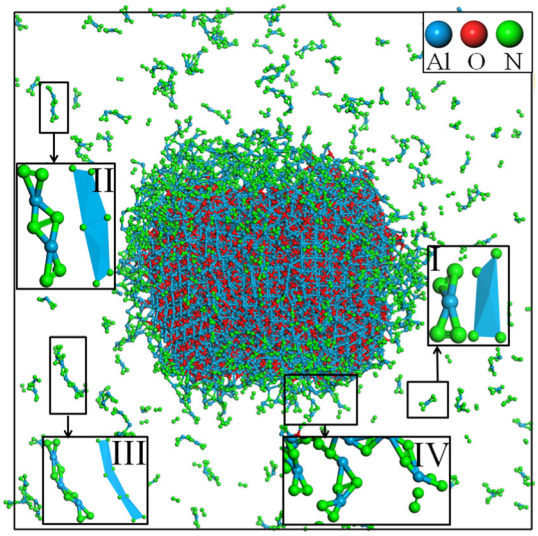

Figure 8 The snapshot of the system at 3500 K with a NO density of 0.15 g/cm^3. The enlarged ball–stick and polyhedron diagrams are AlN_4 (I), Al_2N_6 (II) and Al_3N_8 (III), respectively. The enlarged image (IV) is chain products in surface.

the ambient atmosphere, including AlN_4 (I), Al_2N_6 (II) and Al_3N_8 (III). There are also chain products to be released from the shell.

The presence of chain products promotes the oxidation reaction of ANPs. On the one hand, the n(Al)/m(X) ratio of Al_nX_{2n+2} is greater than that of AlN and Al_4C_3, hence more C and N atoms participate in the reaction. On the other hand, the nanoparticles can provide Al and N atoms for the chain formation reaction. Hence the Al_nX_{2n+2} that ejects from the shell of nanoparticles is more conducive to nucleation and growth, rather than a chain-like product generated in

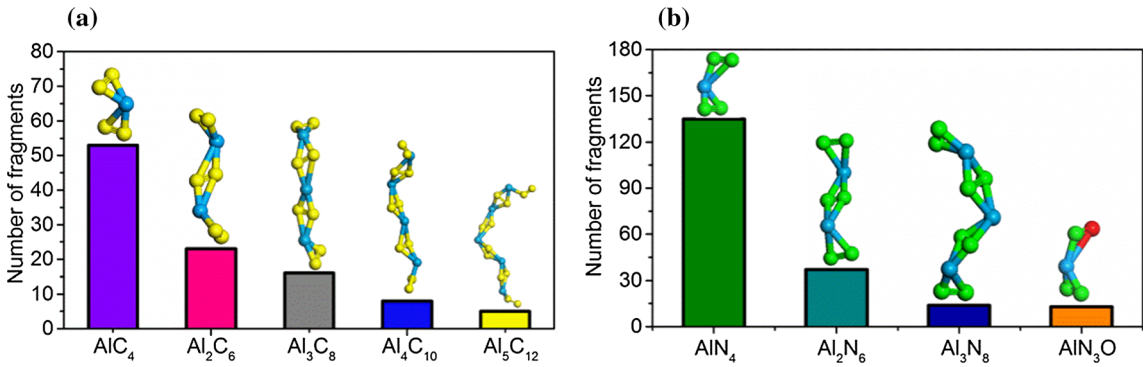

Figure 9 The peak number of chain products in CO atmosphere (**a**) and NO atmosphere (**b**).

the environmental phase. Figure 9 shows the maximum number of various chain products in oxidation reaction. The number of chains decreases as the number of n in Al_nX_{2n+2} increases. For the ANPs–CO and ANPs–NO systems, their maximum n values were observed in the simulations to be 5 and 3, respectively. Although the numbers of AlN_4 and Al_2N_6 (135 and 37, respectively) is more than the number of AlC_4 and Al_2C_6 (53 and 23, respectively), longer C-containing chains appear in CO atmosphere such as Al_4C_{10} and Al_5C_{12}. In addition, a small amount of AlN_3O was detected in the ANPs–NO system. To the best of our knowledge, there has been no research on chain products focused on this oxidation in CO/NO atmosphere. Thus, our results offer new insights into the chain product formation mechanisms.

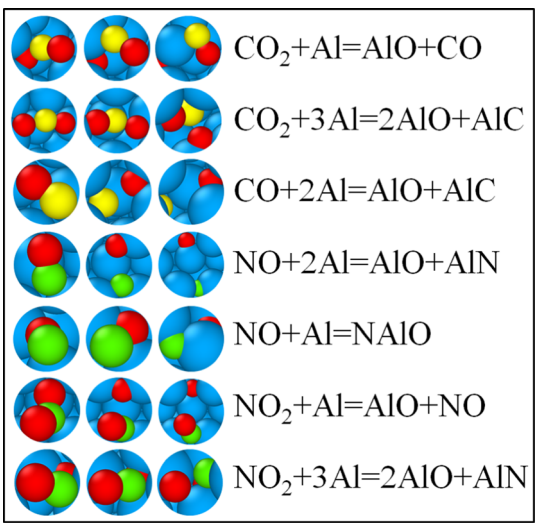

Figure 10 Reaction steps extracted from the initial reaction trajectories of ANPs with different atmospheres.

Initial decomposition pathway of different gas with ANPs

In the initial reaction, the reaction trajectory of gas molecules attacking ANPs is shown in Fig. 10. There are two pathways of CO_2 attacking ANPs. One is that the Al atoms extract an oxygen atom from CO_2 and then the remaining CO is released; the other is that the CO_2 lies flat on the surface of the ANPs and reacts with three Al, and generates 2AlO and AlC. The reaction of NO_2 with ANPs is similar to that of CO_2. When CO attacks the surface of ANPs, AlC and AlO are generated. In addition to the reaction of NO similar to that of CO, it was also observed that with the assistance of another Al, the Al breaks the N–O bond to form NAlO.

Evolution of the potential energy and total species of the system

Evolution of potential energy (PE) of the ANPs–CO_2 system is shown in Fig. 11. The PE curve initially decreases rapidly and then smoothly, indicating a release of energy during CO_2 oxidation. Taking 1500 K as an example, when an equilibrium is reached, the total potential energies released in the CO_2 density of (a) 0.055 g/cm^3, (b) 0.11 g/cm^3, and (c) 0.22 g/cm^3 are 2.412×10^5, 2.575×10^5, and 3.305×10^5 kcal/mol, respectively. The greater the ambient atmosphere concentration, the higher the energy released. Additionally, the higher the temperature, the greater the asymptotic value of PE, indicating that increased temperature accelerates the rate of heat release.

In order to obtain the initial reaction information of the ANPs, a series of C++ scripts were applied to obtain the evolution of the fragments with time. The

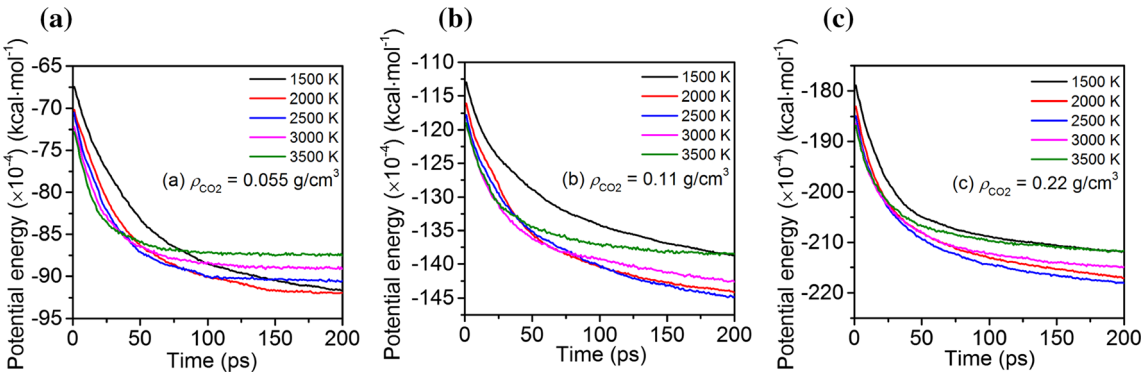

Figure 11 Evolution of PE with CO_2 atmosphere at different temperature. The CO_2 densities of **a** 0.055 g/cm^3, **b** 0.11 g/cm^3, and **c** 0.22 g/cm^3 were selected as examples.

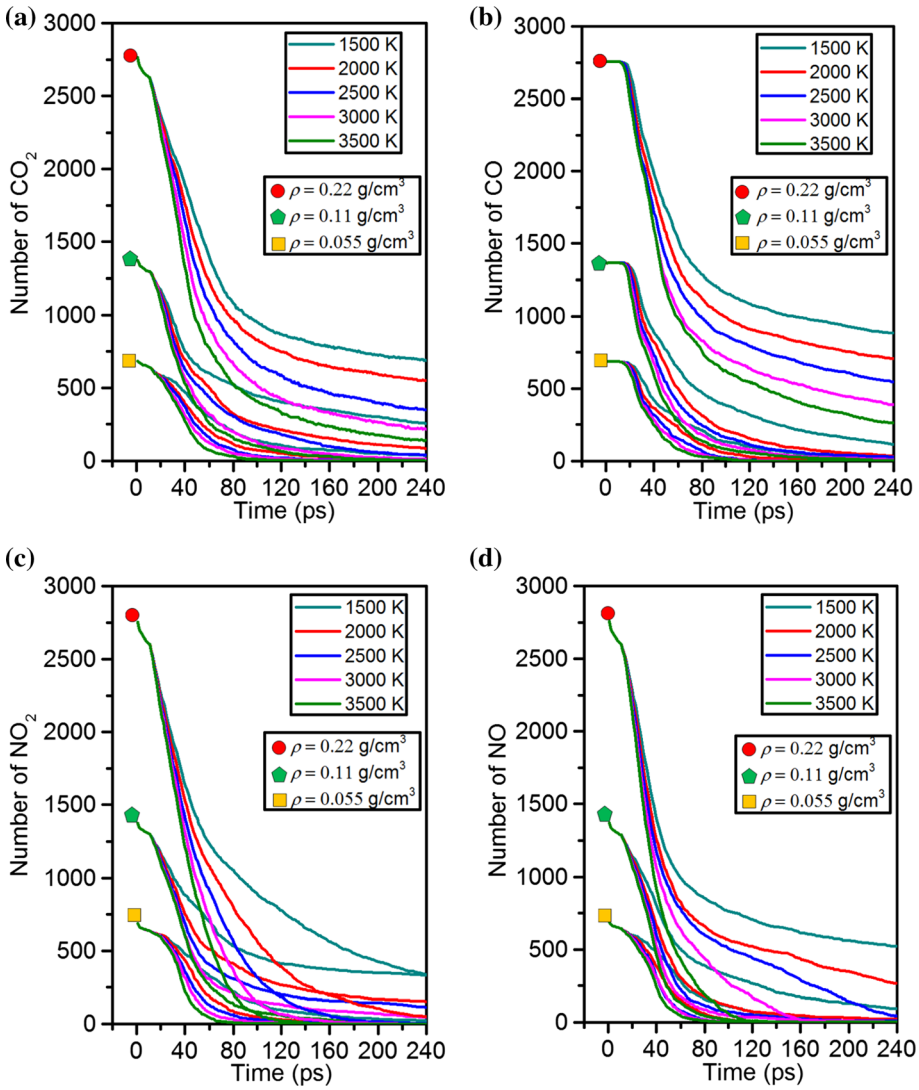

Figure 12 Evolution of CO_2 (**a**), CO (**b**), NO_2 (**c**), and NO (**d**) with time at different temperature.

cutoff bond length is 1.1 times that of the standard single fragment in fragment analysis. Figure 12 shows the reduction of the four gaseous oxides with time. As temperature rises, the number of CO_2, CO, NO_2, and NO shows an accelerated decline, indicating a dependence on temperature. In addition, the

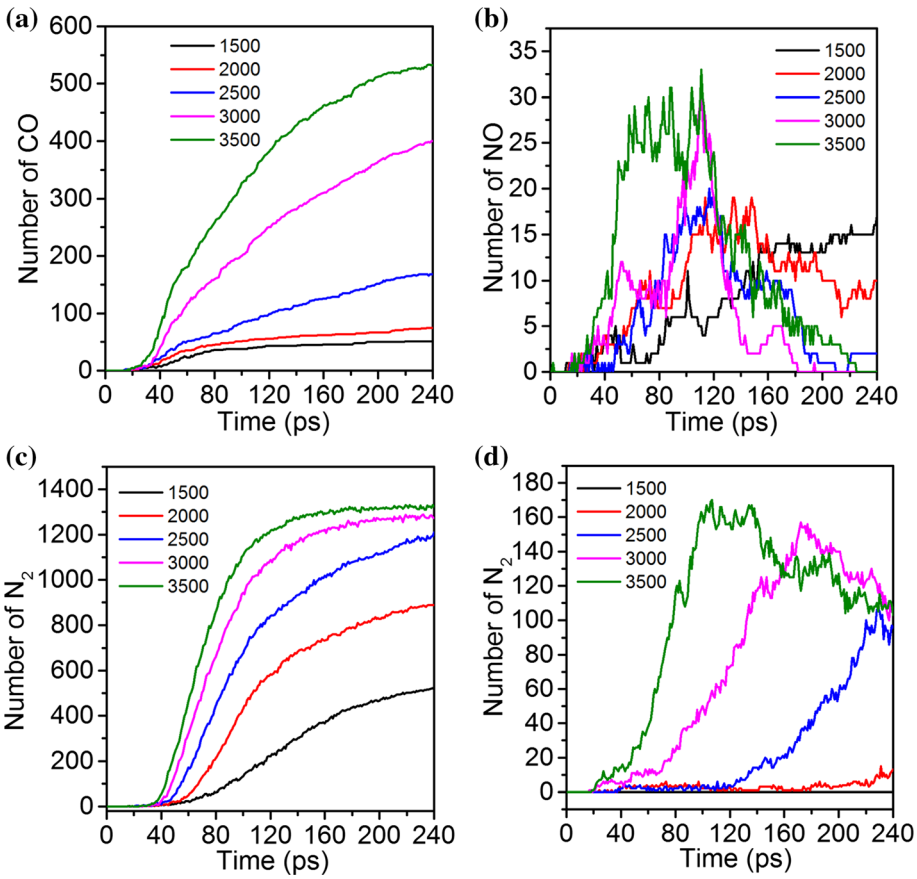

Figure 13 **a** The number of CO gases formed by the CO_2–ANPs system with time at 0.22 g/cm^3. **b** The number of NO gases formed by the NO_2–ANPs system with time at 0.23 g/cm^3. **c** The number of N_2 gases formed by the NO_2–ANPs system with time at 0.23 g/cm^3. **d** The number of N_2 gases formed by the NO–ANPs system with time at 0.15 g/cm^3.

curves of the different densities of NO_2 and NO distinctly intersect with each other. Especially for NO_2, the curves of 0.22 and 0.11g/cm^3 cross at 234 ps, indicating that high density promotes the oxidation of ANPs. CO_2 reacts with ANPs to generate CO during ignition and combustion. Figure 13a shows the number of CO formed at high CO_2 density. CO molecules formed by CO_2 continues to increase from 0 to 240 ps. The higher the temperature, the more CO molecules are formed. NO and N_2 are formed during the ignition and combustion of NO_2 and ANPs. Figure 13b shows the number of NO formed at high NO_2 density. Because NO_2 is more active than CO_2, the amount of NO varies dramatically. At high density, the number of NO molecules initially increases rapidly and then decreases with time. Figure 13c, d shows the number of N_2 formed under NO_2 and NO atmospheres, respectively. For the NO_2 atmosphere, the number of N_2 generated in NO_2 atmosphere slowly rises and then equilibrates. The higher the temperature, the more N_2 is generated. For the NO atmosphere, the number of N_2 rises and then decreases at 2500, 3000 and 3500 K. However, the reaction of ANPs with NO hardly produces N_2 at 1500 and 2000 K. The product evolutions at low1 and medium density are illustrated in Supporting Information (Figure S5 and S6).

Analysis of chemical bonds

The formation of three chemical bonds Al–O, Al–C, and Al–N is the main source of exothermic heat. Therefore, the evolutionary details of these three chemical bonds are helpful to understand the details of the reaction between ANPs and gaseous oxides. Figure 14 shows the evolution of these three chemical bonds with temperature. In CO_2 atmosphere, the amount of Al–O is twice that of Al–C at a low density. With the increase in CO_2 density, the number of Al–O is more than twice that of Al–C. This is because ANPs are more favorable for bonding with O under sufficient CO_2 supply. Due to the formation of carbon-containing chain products and carbon deposition, the number of Al–C slowly decreases at 0.22 g/cm^3 when it reaches its highest peak. In CO atmosphere, the number of Al–O is substantially equal to

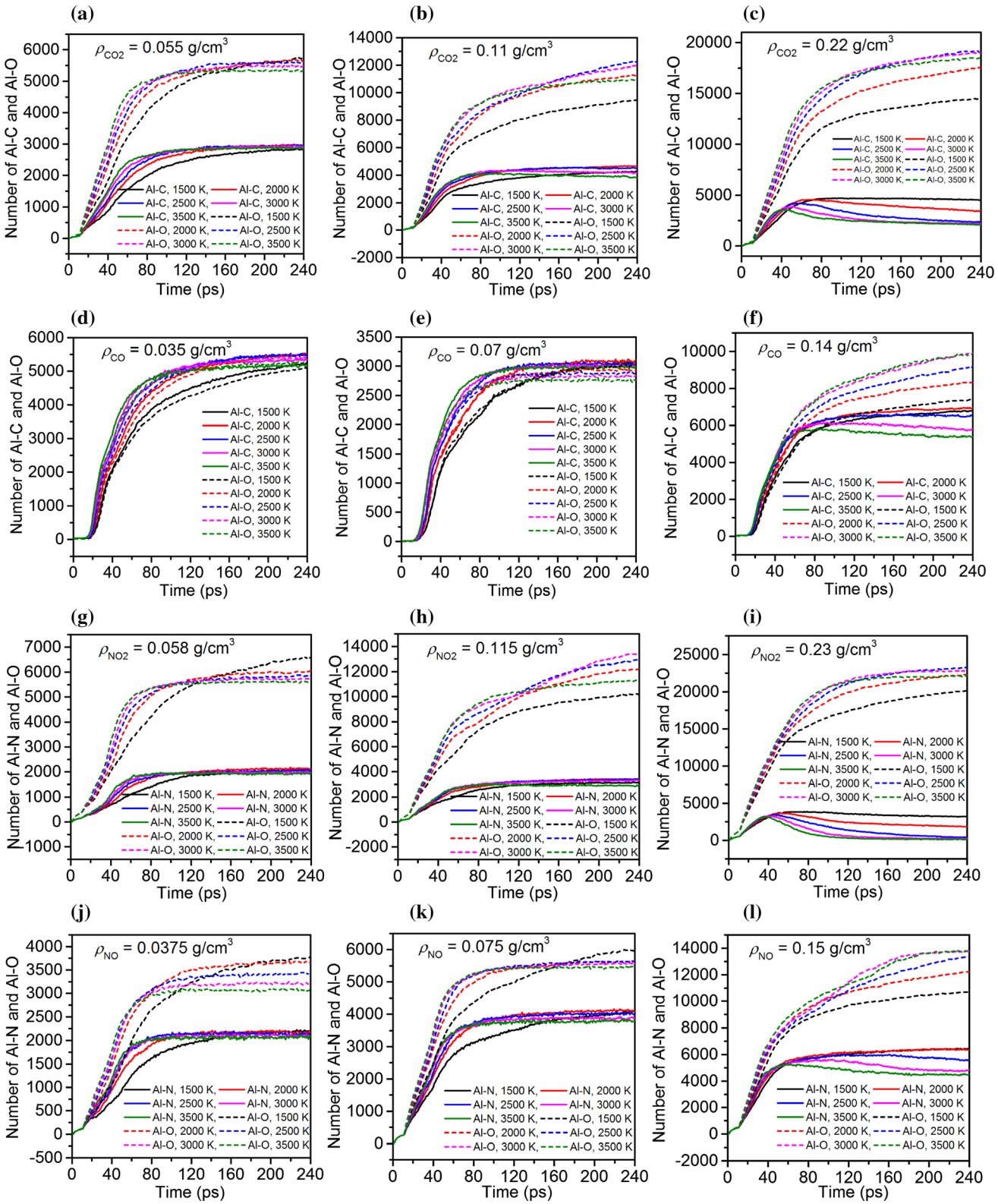

Figure 14 Evolution of Al–O, Al–C, and Al–N with time at different temperature.

the number of Al–C at low density. At 0.14 g/cm^3, the formation of Al–O gradually dominates. This is also because the bonding strength of Al–O is much higher than that of Al–C, hence Al–O is more favorable to be formed when the amount of CO is sufficient. Since N atoms are feasible to form stable N_2, the amount of Al–O is not twice or the same as the amount of Al–N in the nitrogen oxides atmosphere. As shown in Fig. 14g–l, the amount of Al–O is more than three times that of Al–N in NO_2 atmosphere. The amount of Al–O is less than twice that of Al–N in NO atmosphere. In these two nitrogen oxide gases, as the density increases, more amount of Al–O is formed. In addition, under high-density gas, the amount of Al–N also shows a downward trend after reaching the peak similar to the carbon oxides.

Conclusions

In this work, we performed a series of RMD simulations to study the oxidation processes of ANPs in various atmospheres. Based on the morphological evolution of ANPs, the mechanism of surface oxidation, the formation mechanism of chain-like products, and the principle of product void formation are explained during ignition and combustion. Fragment analysis and chemical bonds are further used to analyze changes in reactants, intermediates, and final products. The main results are summarized as follows:

1. The ignition of ANPs in various atmospheres is dependent on the combined effects of temperature and pressure. At the same time, it is also affected by changes in its morphology. In the CO atmosphere, the four forms of chain products include tilted chain, twisted chain, branched chain, and cyclic chain were observed. The chain products are repeatedly arranged in the form of AlC_2, and the head and tail of the chain are C≡C. For the NO atmosphere, a similar chain structure is also formed, but the length of the chain is significantly reduced. The aluminum nitride on the surface enters the environmental phase in chains form when the aluminum oxide phase excludes the aluminum nitride phase at high density.
2. In CO_2 atmosphere, ANPs form an oxide shell and rapidly expand into the outer space, resulting in a void between oxide shell with Al core. Al atoms are transported from the core to the oxide shell through a bridge composed of Al atoms. The Al core gradually diffused outward and was eventually hollowed out. In addition, the final product has carbon deposits (C_{48} and C_{98}) on the surface and core.
3. The analysis of Al–O, Al–C, and Al–N is helpful to understand the details of the reaction between ANPs and gaseous oxides. We found that ANPs ignited and burned Al–O and Al–C in a CO_2 and CO atmosphere at almost 2:1 and 1:1 ratios, respectively. However, the oxidation reaction of ANPs in NO_2 and NO does not show such a rule. This is because N_2 is generated as a stable structure during ignition and combustion compared to nitrogen oxide gas.

Acknowledgements

We thank the Priority Academic Program Development of Jiangsu Higher Education Institutions (PAPD) for supporting this work. L. Song thanks the Innovation Project for Postgraduates in Universities of Jiangsu Province for supporting this work.

Author contributions

Conceptualization was performed by LS and XHJ; data curation was performed by LS; formal analysis was carried out by LS, FQZ, and SYX; project administration was done by XHJ; XHJ carried out supervision; writing of original draft was done by LS; writing, review, and editing was done by XHJ and FQZ.

Compliance with ethical standards

Conflict of interest The authors declare that they have no known competing financial interests or personal relationships that could have appeared to influence the work reported in this paper.

Electronic supplementary material: The online version of this article (https://doi.org/10.1007/s10853-020-05062-y) contains supplementary material, which is available to authorized users.

References

[1] Jayaraman K, Anand KV, Chakravarthy SR, Sarathi R (2009) Effect of nano-aluminium in plateau-burning and catalyzed composite solid propellant combustion. Combust Flame 156:1662–1673

[2] Ao W, Liu P, Liu H, Wu S, Tao B, Huang X, Li L (2020) Tuning the agglomeration and combustion characteristics of aluminized propellants via a new functionalized fluoropolymer. Chem Eng J 382:122987

[3] Griego C, Yilmaz N, Atmanli A (2019) Analysis of aluminum particle combustion in a downward burning solid rocket propellant. Fuel 237:405–412

[4] Kwon YS, Gromov AA, Ilyin AP, Popenko EM, Rim GH (2003) The mechanism of combustion of superfine aluminum powders. Combust Flame 133:385–391

[5] Mench MM, Kuo KK, Yeh CL, Lu YC (1998) Comparison of thermal behavior of regular and ultra-fine aluminum powders (Alex) made from plasma explosion process. Combust Sci Technol 135:269–292

[6] Trunov MA, Schoenitz M, Dreizin EL (2005) Ignition of aluminum powders under different experimental conditions. Propellants Explos Pyrotech 30:36–43

[7] Lerner MI, Glazkova EA, Lozhkomoev AS, Svarovskaya NV, Bakina OV, Pervikov AV, Psakhie SG (2016) Synthesis of Al nanoparticles and Al/AlN composite nanoparticles by electrical explosion of aluminum wires in argon and nitrogen. Powder Technol 295:307–314

[8] Gao J, Yan J, Zhao B, Zhang Z, Yu Q (2020) In situ observation of temperature-dependent atomistic and mesoscale oxidation mechanisms of aluminum nanoparticles. Nano Res 13:183–187

[9] Lade R, Wasewar K, Sangtyani R, Kumar A, Shende D, Peshwe D (2019) Effect of aluminum nanoparticles on rheological behavior of HTPB-based composite rocket propellant. J Energ Mater 37:125–140

[10] Shancita I, Campbell LL, Wu CC, Aquino AJA, Walck SD, Tunega D, Pantoya ML (2019) Effect of hydration on promoting oxidative reactions with aluminum oxide and oxyhydroxide nanoparticles. J Phys Chem C 123:15017–15026

[11] Meda L, Marra G, Galfetti L, Severini F, Luca LD (2007) Nano-aluminum as energetic material for rocket propellants. Mater Sci Eng C 27:1393–1396

[12] Meda L, Marra G, Galfetti L, Severini F, Luca LD (2005) Nano-composites for rocket solid propellants. Compos Sci Technol 65:769–773

[13] Ivanov GV, Tepper F (1997) 'Activated' aluminum as a stored energy source for propellants. Int J Energ Mater Chem Propuls 4:636–645

[14] Zhang YR, van Duin ACT, Luo KH (2018) Investigation of ethanol oxidation over aluminum nanoparticle using ReaxFF molecular dynamics simulation. Fuel 234:94–100

[15] Hong S, van Duin ACT (2015) Molecular dynamics simulations of the oxidation of aluminum nanoparticles using the ReaxFF reactive force field. J Phys Chem C 119:17876–17886

[16] Campbell T, Kalia RK, Nakano A, Vashishta P, Ogata S, Rodgers S (1999) Dynamics of oxidation of aluminum nanoclusters using variable charge molecular-dynamics simulations on parallel computers. Phys Rev Lett 82:4866

[17] Campbell TJ, Aral G, Ogata S, Kalia RK, Nakano A, Vashishta P (2005) Oxidation of aluminum nanoclusters. Phys Rev B 71:205413

[18] Palopoli SF, Brill TB (1991) Thermal decomposition of energetic materials 52. On the foam zone and surface chemistry of rapidly decomposing HMX. Combust Flame 87:45–60

[19] Yan QL, Li XJ, Wang Y, Wang Y, Zhang WH, Zhao FQ (2009) Combustion mechanism of double-base propellant containing nitrogen heterocyclic nitroamines (I): the effect of heat and mass transfer to the burning characteristics. Combust Flame 156:633–641

[20] Nielson KD, van Duin ACT, Oxgaard J, Deng WQ, Goddard WA (2005) Development of the ReaxFF reactive force field for describing transition metal catalyzed reactions, with application to the initial stages of the catalytic formation of carbon nanotubes. J Phys Chem A 109:493–499

[21] Chenoweth K, van Duin ACT, Goddard WA (2008) ReaxFF reactive force field for molecular dynamics simulations of hydrocarbon oxidation. J Phys Chem A 112:1040–1053

[22] Ojwang J, van Santen RA, Kramer GJ, van Duin ACT, Goddard WA (2009) Parametrization of a reactive force field for aluminum hydride. J Chem Phys 131:044501

[23] van Duin ACT, Strachan A, Stewman S, Zhang Q, Xu X, Goddard WA (2003) $Reaxff_{sio}$ reactive force field for silicon and silicon oxide systems. J Phys Chem A 107:3803–3811

[24] Ashraf C, Vashisth A, Bakis CE, van Duin ACT (2019) Reactive molecular dynamics simulations of atomic oxygen impact on epoxies with different chemistries. J Phys Chem C 123:15145–15156

[25] Wang N, Peng J, Pang A, He T, Du F (2017) Thermodynamic simulation of the RDX–aluminum interface using ReaxFF molecular dynamics. J Phys Chem C 121:14597–14610

[26] Nosé S (1984) A unified formulation of the constant temperature molecular dynamics methods. J Chem Phys 81:511–519

[27] Hoover WG (1985) Canonical dynamics: equilibrium phase-space distributions. Phys Rev A 31:1695

[28] Plimpton S (1995) Fast parallel algorithms for short-range molecular dynamics. J Comput Phys 117:1–19

[29] Chakraborty P, Zachariah MR (2014) Do nanoenergetic particles remain nano-sized during combustion? Combust Flame 161:1408–1416

[30] Bucher P, Yetter RA, Dryer FL, Vicenzi EP, Parr TP, Hanson-Parr DM (1999) Condensed-phase species distributions about Al particles reacting in various oxidizers. Combust Flame 117:351–361

[31] Brandstadt K, Frost DL, Kozinski JA (2009) Preignition characteristics of nano-and micrometer-scale aluminum particles in Al–CO_2 oxidation systems. P Combust Inst 32:1913–1919

[32] Zhang X, Fu C, Xia Y, Duan Y, Li Y, Wang Z, Jiang Y, Li H (2019) Atomistic origin of the complex morphological evolution of aluminum nanoparticles during oxidation: a chain-like oxide nucleation and growth mechanism. ACS Nano 13:3005–3014

[33] Sarou-Kanian V, Rifflet JC, Millot F, Gökalp I (2006) Aluminum combustion in wet and dry CO_2: consequences for surface reactions. Combust Flame 145:220–230

[34] Shafirovich E, Varma A (2008) Metal-CO_2 propulsion for mars missions: current status and opportunities. J Propuls Power 24:385–394

[35] Li G, Niu L, Hao W, Hao W, Liu Y, Zhang C (2020) Atomistic insight into the microexplosion-accelerated oxidation process of molten aluminum nanoparticles. Combust Flame 214:238–250

[36] Sarou-Kanian V, Rifflet J, Millot F, Matzen G, Gökalp I (2005) Influence of nitrogen in aluminum droplet combustion. Proc Combust Inst 30:2063–2070